EURASIAN PHYSICAL TECHNICAL JOURNAL

2024, Volume 21, No.3 (49)

https://doi.org/10.31489/2024No3/6-20

Received: 03/04/2024 Revised: 26/06/2024 Accepted: 06/09/2024 Published online: 30/09/2024

Research Article

UDC 539.199, 544.723.2

CONFORMATIONAL STRUCTURE OF POLYAMPHOLYTES AND POLYELECTROLYTES ON THE SURFACE OF A LONGITUDINALLY POLARIZED GOLD SPHEROCYLINDER

Kucherenko M.G., Kruchinin N.Yu.*, Neyasov P.P.

Center of Laser and Informational Biophysics, Orenburg State University, Orenburg, Russia

*Corresponding author: *kruchinin_56@mail.ru

Abstract. *Conformational changes in generally neutral polyampholytic, as well as uniformly charged macrochains, polypeptides adsorbed on the surface of a longitudinally polarized gold spherocylinder—a cylindrical nanorod with spherical ends—were studied. An analytical model of the equilibrium structure of adsorbed macrochains on the surface of a polarized spherocylinder is presented, highlighting the entropy and field factors of the radial-angular distribution of link density. In the course of molecular dynamics simulation, the radial distributions of the density of polypeptide atoms in the central cylindrical part of the nanorod, as well as on its terminal hemispheres, were calculated. In addition, the distributions of the linear density of polypeptide atoms along the axis of the nanorod were calculated. A dumbbell-shaped polyampholyte edge was formed on the surface of the polarized nanorod, dense in the extended central cylindrical part and loose at the ends of the nanorod. There was also a shift of the macromolecular edge from the units of a uniformly charged polypeptide to the oppositely charged end of the nanorod, on which this polyelectrolyte edge swelled.*

Keywords: gold nanorod, polarized nanoparticle, polyampholyte, polyelectrolyte, conformational structure, molecular dynamics

1. Introduction

Currently, gold nanorods or nanospheroids that form conjugates with biopolymers are widely used in the creation of functional elements of various chemical sensors based on the effects of Förster energy transfer between nanoobjects connected by a macrochain and giant Raman scattering, as well as in the creation of nanostructured materials with embedded gold nanoparticles [1-13]. Of great interest in this case is the control of the characteristics of such nanosystems by changing the conformational structure of the adsorbed macrochain under the influence of an external electric field. In this case, it is necessary to use polyelectrolyte macromolecules that contain charged units, or polyampholytes, with electric dipole moments of monomers or unit fragments in their structure as such macrochains.

Previously, the authors in a number of works [14–22] studied electrically induced changes in the conformational structure of generally neutral polyampholytes or uniformly charged polyelectrolyte macrochains on the surface of a cylindrical gold nanowire transversely polarized in an external electric field, as well as an elongated or oblate gold nanospheroid polarized along the major axis. However, when creating such hybrid nanosystems, rather short cylindrical gold nanorods, the ends of which are spherical or spheroidal surfaces, are often used [1-13]. Such nanorods in some cases can be approximately considered as elongated nanospheroids with the length of the major axis equal to the length of the nanorod and the length

of the minor semi-axes equal to the radius of the nanorod. However, in the case of longitudinal polarization of such a nanorod in an external electric field, the distribution of induced charges on its surface will differ significantly from the distribution of induced charges on the surface of an elongated metal nanospheroid polarized along the major axis. On the surface of the cylindrical part of a metal nanorod, if it is longitudinally polarized, the surface density of induced electric charges will be zero, and all induced charges will be concentrated only at its ends. In particular, if the ends of the nanorod have a spherical surface shape, then the charges induced by the external electric field will be distributed according to the cosine law between the direction of the electric field and the normal to the surface [23]. This distribution of surface charges will have a significant impact on the conformational structure of polyelectrolytes adsorbed on the surface, which will vary significantly depending on the strength of the external polarizing electric field.

On the other hand, as was shown in [22], the formed conformational structure of the edge will also be influenced by the curvature of the adsorbing surface of the nanoparticle through the entropy factor. The radial distribution of the density of uncharged chain links on the cylindrical section of the particle has a different character than the similar distribution at the surface of the nanosphere.

Thus, the goal of this work is to study the conformational structure of generally neutral polyampholyte and uniformly charged polyelectrolyte macrochains on the surface of a longitudinally polarized cylindrical gold nanorod with spherical ends.

2. Mathematical model of the conformational structure of polyampholyte and polyelectrolyte chains on the surface of a spherocylinder polarized in an electric field

In [19, 22], the formation of an openwork structure of a polyampholyte macrochain (edge) adsorbed on the surface of nanoparticles of various shapes (spheres, spheroids, cylinders) was considered on the basis of a generalized model of an ideal Gaussian chain interacting with an adsorbent particle through two potential fields: van- der Waals $V(\mathbf{r})$ and electric, arising in addition to $V(\mathbf{r})$ as a result of polarization of the nanoparticle by an external field of intensity $\mathbf{E_0}$.

The configuration function $\psi(\mathbf{r})$ of an ideal Gaussian macrochain (i.e. a chain without bulk inter-link interactions) in the potential van der Waals field $V(\mathbf{r})$ of the adsorbent surface satisfies an equation that is isomorphic to the stationary Schrödinger equation [24]:

$$\frac{a_0^2 kT}{6}\nabla^2\psi(\mathbf{r}) = [V(\mathbf{r}) - \varepsilon]\psi(\mathbf{r}) \cdot \tag{1}$$

Here, in (1) a_0 is the length of the chain link, kT is the thermal energy at temperature T of the system, and ε is a constant with the dimension of energy (eigenvalue of the Grosberg-Khokhlov operator). Surfaces of constant density of monomer units of a polymer reflect the geometry of the adsorbing boundary, therefore, to write equation (1) in the case of a spherocylinder, cylindrical and spherical coordinate systems were used simultaneously, with each section of the composite particle having its own. The conformational function $\psi(\mathbf{r})$, depending on the radius vector $\mathbf{r}$ of the unit, found by solving equation (1), makes it possible to take into account the entropy aspects of the formation of various conformations of the adsorbed macrochain. Thus, the spatial distribution of the local density of chain links $n(\mathbf{r})$ is determined by the square of the conformational function corresponding to the minimum eigenvalue ε_0: $n_0(\mathbf{r}) = \psi_0^2(\mathbf{r})$ [24]. In the case of a quasi-stationary electric field of strength $E(t)$, one can consider quasi-equilibrium conformations of a macromolecule adsorbed on a nanoparticle, as was done, for example, in [20].

The energy of the additional (in addition to $V(\mathbf{r})$) interaction of the electric field of a nanoparticle with a separate link, or a group of polyampholyte links with a characteristic electric dipole moment $\mathbf{p}$ of a separate selected segment (a single link or a group of links) can be written in the form

$$V_{\mathbf{p}}^{(e)}(\mathbf{r}) = -\mathbf{p}\nabla\varphi^{(e)}(\mathbf{r}) \cdot \tag{2}$$

For a polyelectrolyte carrying a charge q on an individual chain link, the additional interaction energy

$$V_q^{(e)}(\mathbf{r}) = q \cdot \varphi^{(e)}(\mathbf{r}) \cdot \tag{2'}$$

The resulting equilibrium spatial distribution of the density $n(\mathbf{r})$ of macrochain units of a polyampholyte or polyelectrolyte adsorbed by a polarized nanoparticle in the approximation of the independent action of entropy and force factors [22] can be represented by the Boltzmann exponent:

$$n(\mathbf{r}) = \psi_0^2(\mathbf{r}) \exp\left[-\frac{V_{\mathbf{p}(q)}^{(e)}(\mathbf{r})}{kT} \right]. \tag{3}$$

The entropy factor $\psi_0^2(\mathbf{r})$ in (3) contains information about the linear memory of the polymer, as well as the features of the curvature of the surface of the adsorbing nanoparticle and its Van de Waals potential $V(\mathbf{r})$. The second, Boltzmann factor for the potential field $V_{\mathbf{p}(q)}^{(e)}(\mathbf{r})$, reflects the result of the action of the quasi-static field (2) or (2') within the framework of the independent links model. The role of this factor in the formation of macrochain conformations during its adsorption on a polarized elongated spheroidal nanoparticle in an external field was studied by us earlier in [19].

To determine the entropy factor $\psi_0^2(\mathbf{r})$ for a spherocylinder in (3), as in the case of a compressed spheroid [22], the solution to equation (3) can be represented by a simple analytical expression obtained for a composite figure of a circular cylinder with two hemispheres ("stubs" of radius $R=b=c$, where b and c are the minor semi-axes of the prolate spheroid).

Previously, in [14, 16], the radial dependences of the concentration of units were determined for cylindrical and spherical nanoparticles with δ-functional well simulating the attraction of units of a polymer molecule to the surface of the nanoparticle.

Then, for the cylindrical part of a composite model nanoparticle with radius $R=b=c$, i.e. in the region $-L/2 \le z \le L/2$ (L - length of the cylindrical part) the solution of equation (1) with a potential in the form of a delta-functional well and a solid wall

$$V(r) = \begin{cases} -\alpha\delta(r - r_0), & r > R \\ V_\infty(r) = \infty, & r = R \end{cases} \tag{4}$$

can be written in the form

$$\begin{cases} \psi_I = A\left(I_0(qr) - K_0(qr)\dfrac{I_0(qR)}{K_0(qR)} \right), & R < r < r_0 \\ \psi_{II} = AK_0(qr)\left(\dfrac{I_0(qr_0)}{K_0(qr_0)} - \dfrac{I_0(qR)}{K_0(qR)} \right) & r_0 < r < \infty \end{cases}, \tag{5}$$

where I_0 and K_0 are the Bessel functions of the imaginary argument of the zero order of the first and second kind, respectively, A is a constant, and the parameter q is found from the solution of the transcendental equation:

$$K_0(qr_0)I_0(qr_0) = \frac{a_0^2 kT}{6\alpha r_0} + K_0^2(qr_0)\frac{I_0(qR)}{K_0(qR)}. \tag{6}$$

The solution to Grosberg-Khokhlov equation (1) [24] with the delta-functional potential (4) of attraction at radius r_0 and the repulsive wall $V_1(r) = V_\infty(R) - \alpha\delta(r - r_0)$, where α - depth of well, on the surface of the nanoparticle for a spherical nanoparticle of radius R has the form ($A=const$)

$$\begin{cases} \psi_I(r) = A\left[\dfrac{I_{1/2}(qr)}{\sqrt{r}} - \dfrac{I_{1/2}(qR)}{K_{1/2}(qR)}\dfrac{K_{1/2}(qr)}{\sqrt{r}} \right], & R < r < r_0 \\ \psi_{II}(r) = A\left[\dfrac{I_{1/2}(qr_0)}{K_{1/2}(qr_0)} - \dfrac{I_{1/2}(qR)}{K_{1/2}(qR)} \right]\dfrac{K_{1/2}(qr)}{\sqrt{r}}, & r_0 < r < \infty \end{cases}, \tag{7}$$

where the parameter q is the root of the equation

$$\frac{a_0^2 kT}{6\alpha r_0} = I_{1/2}(qr_0)K_{1/2}(qr_0) - K_{1/2}^2(qr_0)\frac{I_{1/2}(qR)}{K_{1/2}(qR)}. \quad (8)$$

Spherically symmetric functions (7) are represented through the Bessel functions $I_{1/2}(qr)$ and $K_{1/2}(qr)$ the imaginary argument with index 1/2. Using (7), it is easy to represent the conformational functions on the surfaces of two stub hemispheres $L/2 \le z \le L/2 + R$ and $-L/2 - R \le z \le -L/2$, similar to how it was done for a compressed spheroid in [22].

Then the spatial distribution (3) of the density $n(\mathbf{r})$ of macrochain units adsorbed by a polarized nanoparticle takes the form

$$n(\mathbf{r}) = \left\{ \begin{matrix} \psi_I^2(r,z), & R < r < r_0 \\ \psi_{II}^2(r,z), & r_0 < r < \infty \end{matrix} \right\} \exp\left[-\frac{V_{\mathbf{p}(q)}^{(e)}(\mathbf{r})}{kT} \right]. \quad (3')$$

The entropy factor $\psi_{I,II}^2(\mathbf{r})$ in the form of the square of conformational functions (5) or (7) is used to describe the density of units in different sections of the spherocylinder: two hemispheres or a central cylindrical insert.

Approximation of the electric field of a spherocylinder by a prolate spheroid

The characteristics of the electric field of a spherocylinder can be described with acceptable accuracy by replacing a cylinder with two spherical ends of a radius $R=b=c$ with an elongated spheroid with similar geometric parameters (Fig. 1). Then the semimajor axis of the spheroid automatically determines the length L of the cylindrical part of the figure: $a=R+L/2>b$. The potential of the resulting field outside a conducting spheroid polarized in an alternating external uniform field parallel to its major axis a with the vector $\mathbf{E}_0$ oriented along the x axis can be written in the following form [23]:

$$\varphi^{(e)} = -E_0 x \times$$
$$\times \left\{ 1 - \frac{[\varepsilon(\omega) - \varepsilon^{(e)}]}{\left\{\varepsilon^{(e)} + [\varepsilon(\omega) - \varepsilon^{(e)}]n^{(x)}\right\}} \frac{(1-e^2)}{2e^3} \left[\ln \frac{\sqrt{1+\xi_1/a^2} + e}{\sqrt{1+\xi_1/a^2} - e} - \frac{2e}{\sqrt{1+\xi_1/a^2}} \right] \right\}. \quad (9)$$

$$\varphi_0 = -E_0 x = -E_0 \xi\eta \frac{d^2}{4\sqrt{a^2-b^2}} = -E_0 \eta \frac{d}{2} \frac{\sqrt{(\xi_1 + a^2)}}{\sqrt{a^2-b^2}}. \quad (10)$$

Here, to describe the field of charged and polarized axisymmetric ellipsoidal bodies (ellipsoids of revolution, for which semi-axes $b=c$) ellipsoidal coordinates are used $\xi_1 = (r_1 + r_2)^2/4 - a^2$, $\eta_1 = (r_1 - r_2)^2/4 - a^2$, φ, where are the focal radii and the eccentricity of the prolate spheroid $e = \sqrt{1 - b^2/a^2}$. For points on the surface of a spheroid ξ_1=0.

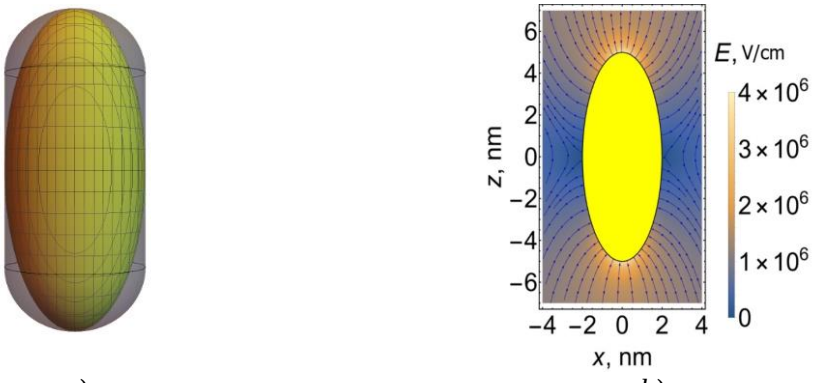

a) *b)*

Fig.1. Spherocylinder and its approximation by an elongated spheroid (a), distribution of electric field strength outside the spheroid (b).

In an alternating electric field that varies harmoniously with frequency ω, the metal nanoparticle is characterized by a dielectric constant $\varepsilon(\omega)$. In (9), the frequency dispersion of the dielectric constant $\varepsilon(\omega)$ of a metal in the form of a Drude-Lorentz is taken into account [23]. The dielectric constant of the external medium $\varepsilon^{(e)}$ is assumed to be constant.

In the model presented above, as in [19, 22], the adsorption van der Waals potential $V(\mathbf{r})$ of the surface of an uncharged spheroidal nanoparticle can be specified by a combination (4) of the simplest model potentials "solid wall – delta functional well".

3. Simulation results

Based on expressions (2 – 10), calculations were made of the field characteristics in the vicinity of a gold spherocylinder (total length 10 nm, radius of the cylindrical part and two hemispheres 2 nm) and the density of units of a macrochain of a polyelectrolyte or polyampholyte type adsorbed on it. The magnitude of the charge of the link or its dipole moment, the strength of the polarizing field, as well as the depth and position of the van der Waals well were varied, along with the temperature, the dimensions of the links and the lengths of the semi-axes of the spherocylinder.

Figure 1a shows the approximation of a spherocylinder by an elongated spheroid. And Figure 1b shows a picture of the field strength of an elongated polarized spheroid. It is more convenient to calculate the field characteristics by imagining the nanoparticle in the form of an elongated spheroid, so formulas (9) and (10) were used for this.

In Fig. 2 shows the concentration distributions of polyelectrolyte units near the surface of an uncharged polarized nanorod with hemispherical ends for different values and signs of charge q of the chain link: -0.1|*e*| (Fig. 2a and 2d), 0 (Fig. 2b and 2e), 0.1|e| (Figure 2c and 2f) taking into account the entropy factor $\psi_0^2(\mathbf{r})$ and Boltzmann factor factors $W(\mathbf{r}) = \exp\left[-V^{(e)}_{\mathbf{p}(q)}(\mathbf{r}) / kT\right]$ based on formula (3'). Simulation parameters: a =5nm, b=c=2nm (radius of the cylinder and hemispheres), α=5·10^{-3} eV·nm (potential well depth), a_0=0.5 nm (link length), temperature T=300 K, E_0=106 V/cm. The figure shows that for a macrochain with neutral links (Figs. 2b and 2e), monomers on the surface of a spherocylinder polarized in an external electric field are distributed uniformly throughout, since the macromolecule is not sensitive to the effect of an electric field.

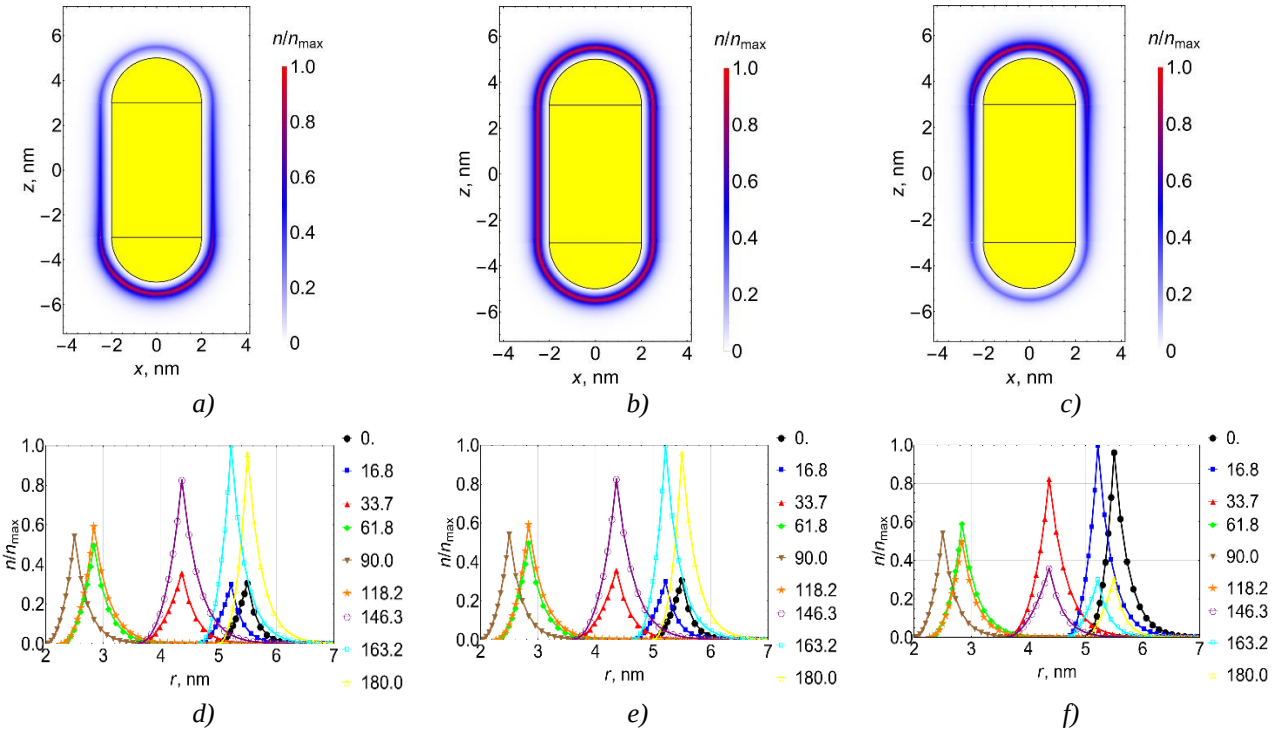

Fig.2. Distribution of the concentration of polyelectrolyte units near the surface of a polarized nanorod for different values and signs of the unit charge: -0.1|e| (a, d), 0 (b, e), 0.1|e| (c, f). Figures d, e, f show the angular distributions of unit concentrations from the center of the nanoparticle (angle 0 degrees is the direction along the external electric field strength vector, and angle 180 degrees is in the opposite direction).

And when the sign of the polyelectrolyte link charge changes, a mirror image of displaced monomers is observed on the surface of the spherocylinder (Figs. 2a and 2c), as well as the corresponding curves of the distributed concentration of the units in different directions (Figs. 2d and 2f).

When the localization radius r_0—the position of the delta-functional van der Waals well—changed from r_0=2.3 nm to r_0=2.7 nm, the radial-angular density distributions (3) changed noticeably both at the end sections of the nanoparticle and in the region of the cylindrical section.

Thus, the contribution of the van der Waals interaction, represented by the delta function, is felt when the radius of its action zone changes. The parameter α, which determines the effective depth of the van der Waals well, manifests itself in a similar way. Temperature T and the length of the macrochain link a_0 are included in (1) in the form of a product, therefore the influence of these parameters on the distribution picture should be considered together. Analysis of the calculated curves showed that an increase in the parameter a_0T levels out the difference in the amplitudes of the radial distributions at different ends of the spherocylinder

Figure 3 shows the pattern of changes in polyelectrolyte links on the surface of a spherocylinder at different values of the external electric field. It is evident that with an increase in the electric field strength from E_0=10^5 V/cm (Fig. 3a) to E_0=3 10^6 V/cm (Fig. 3c), a significant shift of the macrochain monomers to the oppositely charged end of the nanoparticle is observed. This is clearly seen in the graphs of the angular distributions of the link concentration (Fig. 3, d-f). At the lowest value of the external electric field strength (Fig. 3d) in any direction from the center of the nanoparticle, the peaks of the monomer concentration distributions are at the same level. And as the external electric field strength increases (Fig. 3, e and f), the peaks of the link concentration become lower and lower, the larger the angle.

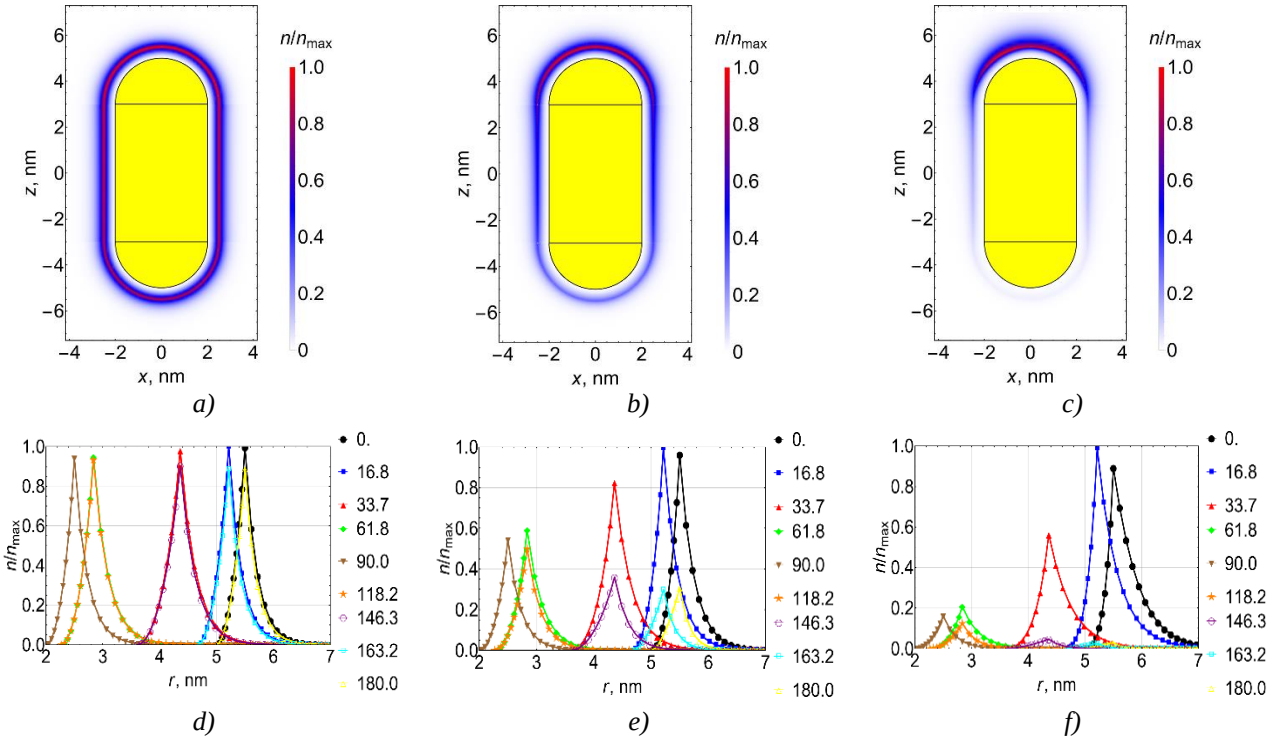

Fig.3. Distribution of the concentration of polyelectrolyte units (unit charge q=0.1|e|) at different values of the polarizing field strength E_0: 10^5 V/cm (a, d), 10^6 V/cm (b, e), 3 10^6 V/cm (c, f). Figures d, e, and f show the angular distributions of unit concentrations from the center of the nanoparticle.

The degree of elongation of the nanoparticle (Fig. 4) also significantly affects the distribution of monomer density: it, as expected, has the least pronounced angular dependence for a sphere, and a more pronounced one for a nanoparticle with a relatively large cylindrical part. With a proportional change in the radii of the cylinder and hemispheres, the angular dependences appear more noticeable for nanoparticles with a large radius. In Figure 4d, corresponding to the sphere (Fig. 4a), the smallest difference between the curves of the monomer concentration distributions in opposite directions is observed. With increasing elongation of the spherocylinder (Fig. 4, b and e) and even stronger elongation (Fig. 4, c and f), an increasingly greater

difference is observed between the curves of the angular distributions of the monomer concentration in the lower half of the spherocylinder (angles from 90 to 180 degrees) and the upper (angles from 0 to 90 degrees).

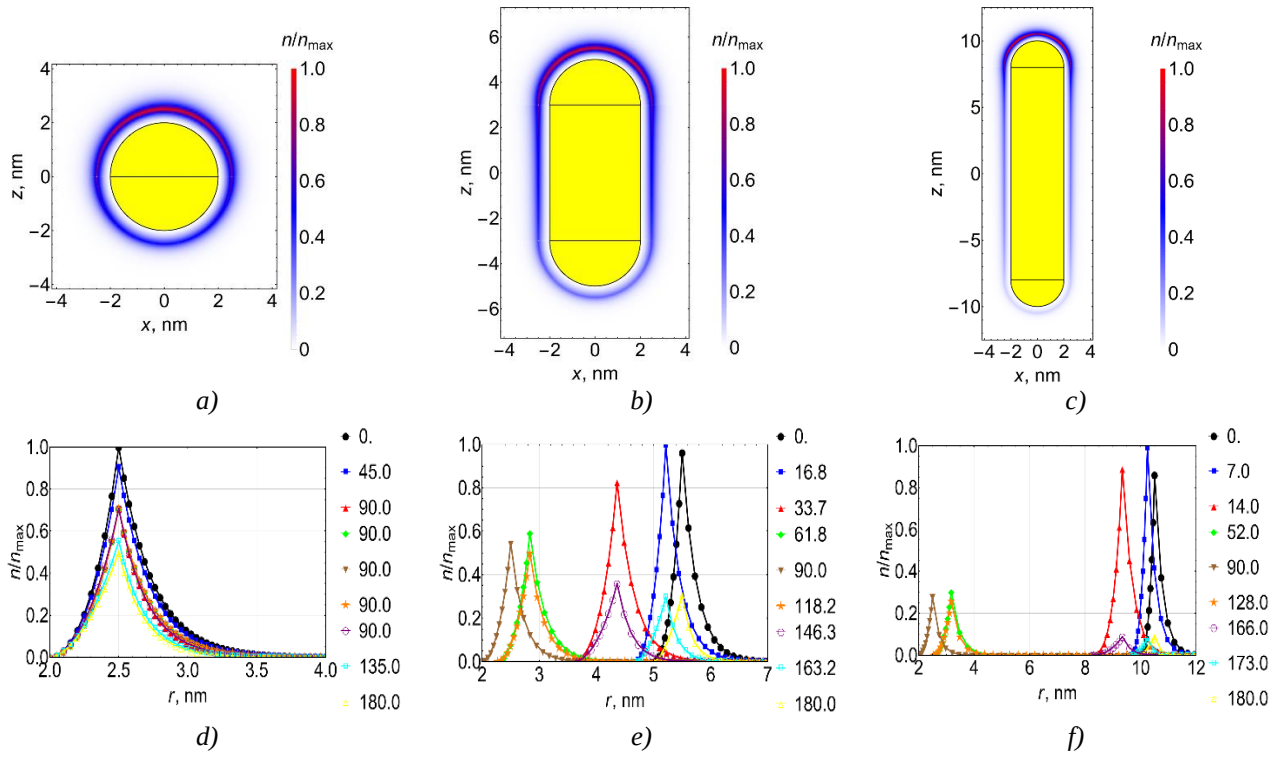

Fig.4. Distribution of the concentration of polyelectrolyte units (unit charge q=0.1|e|) for different lengths of the cylindrical part of the nanorod b=c=2 nm: a=2 nm (a, d), a=5 nm (b, e), a=10 nm (c, f). Figures d, e, and f show the angular distributions of unit concentrations from the center of the nanoparticle.

In Fig. 5 shows the distribution of the concentration of polyampholyte units in a longitudinal electric field of different strengths E_0, taking into account entropy and field factors together in the presence of a dipole moment at link $\boldsymbol{p}$ of the macrochain. Both factors (entropy and Boltzmann) are taken into account together in expression (3'), the reference point is at the center of the nanoparticle, on its axis. Values of modeling parameters used in the calculation, E_0=10^5-3 10^6 V/cm, a=5 nm, b=c=2 nm, α=5·10^{-3} eV·nm, r_0=R+0.5 nm, R=b=c (radius of the cylinder and both hemispheres), a_0=0.5 nm (link length), T=300 K. Significant differences are observed in the angular dependences of the distribution of polyampholyte units from the case of polyelectrolyte. Firstly, there is a symmetry of the angular density distribution associated with the free reorientation of the dipole p of the chain link in the field. Secondly, the lowest density of units is formed in the middle section passing through the origin at the center of the nanoparticle. The shift in the van der Waals well localization zone is not as noticeable as in the case of a polyelectrolyte. The same applies to the parameter of the effective depth of the van der Waals well. An increase in the a_0T (1) parameter leads to a leveling of the amplitudes of the radial distributions for different angles – as in the case of a polyelectrolyte. In a weak electric field, the anisotropy of the distribution is not pronounced, and the radial dependence of the density is entirely formed by the van der Waals field. However, in a field of E_0 = 3 10^6 V/cm, a strong shift in the density of the chain monomers to both ends of the nanoparticle is observed. Stretching the spherocylinder, that is, lengthening its cylindrical part, leads to an increase in the degree of anisotropy in the distribution.

A change in the radius r_0 of the delta-functional well localization from r_0=2.3 nm to r_0=2.7 nm leads to a noticeable change in the radial-angular distributions of the polyampholyte density (3) both at the end sections, i.e. in the region of hemispheres and in the region of the cylindrical section. The contribution of the van der Waals interaction to the pattern of link distribution should be recognized as significant, because it is transformed when the parameter α, which determines the effective depth of the van der Waals well, changes. The product of temperature and the length of the macrochain link a_0T affects the difference in the amplitudes of the radial distributions in the cylindrical part and at the ends of the spherocylinder.

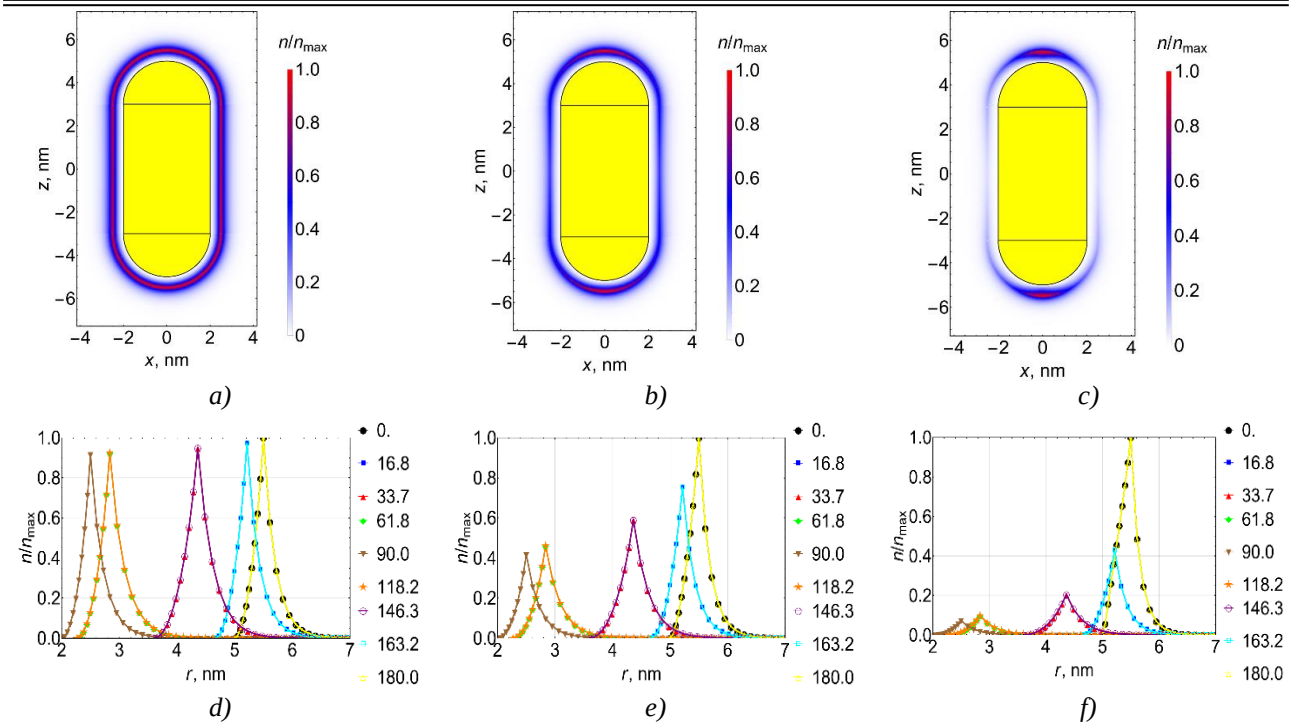

Fig.5. Concentration distribution of polyampholyte units (unit dipole moment 5 D) in a longitudinal electric field of strength E_0: 10^5 V/cm (a, d), 10^6 V/cm (b, e) 3 10^6 V/cm (c, f). Figures c, d show the angular distributions of unit concentrations from the center of the nanoparticle.

A relative increase in the length of the cylindrical part of the spherocylinder (Fig. 6) leads to the effect of depletion of the density of links in the central zone and enrichment of the density at the ends. A proportional change in the radii and length of the central part of the sphero-cylinder does not lead to the same noticeable effect of redistribution of monomer density, but gives a smoother differentiation.

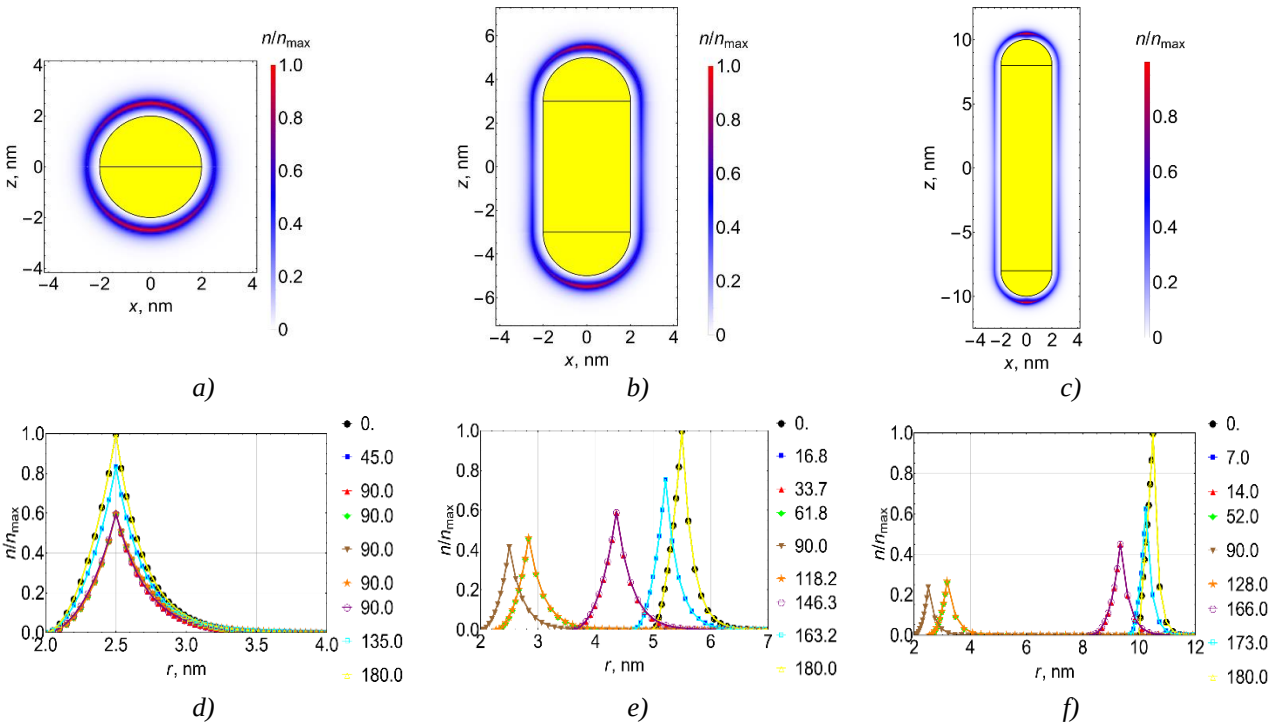

Fig.6. Distribution of the concentration of polyampholyte units (unit dipole moment 5 D) for different lengths of the cylindrical part of the nanorod b=c=2 nm: a=2 nm (a, d), a=5 nm (b, e) a=10 nm (c, f). Figures d, e and f show the angular distributions of unit concentrations from the center of the nanoparticle.

4. Initial data for molecular dynamics simulation, features of its implementation and processing

Molecular dynamics (MD) simulation of polypeptides on the surface of a gold nanorod was carried out using the NAMD 2.14 software package [25]. A model of a gold nanorod was obtained by cutting out a gold crystal: the central part of a cylindrical nanorod with a length of about 6 nm and a radius of 1.5 nm, and two hemispheres with a radius of 1.5 nm were located at the ends. During the MD simulation, the atoms of the nanorod remained fixed.

Three generally neutral polyampholytic polypeptides were considered:

1) polypeptide **P1**, consisting of 600 amino acid residues with 480 Ala (A) units with evenly distributed 60 Asp units (D, charge -1*e*) and 60 Arg units (R, charge +1*e*) – $(A_2DA_4RA_2)_{60}$;

2) polypeptide **P2**, consisting of 980 amino acid residues with 784 Ala units with evenly distributed 49 pairs of Asp units and 49 pairs of Arg units– $(A_4R_2A_8D_2A_4)_{49}$;

3) polypeptide **P3**, consisting of 988 amino acid residues with 880 Ala units with evenly distributed 27 pairs of Asp units and 27 pairs of Arg units– $A_8(A_8D_2A_{16}R_2A_8)_{27}A_8$.

Three uniformly negatively charged polypeptides consisting of 800 amino acid residues were also considered:

4) polypeptide **P4** (total macrochain charge -40*e*), consisting of 760 Ala units with 40 Asp units evenly distributed– $(A_{10}DA_9)_{40}$;

5) polypeptide **P5** (total macrochain charge -80*e*), consisting of 720 Ala units with 80 Asp units evenly distributed– $(A_5DA_4)_{80}$;

6) polypeptide **P6** (total macrochain charge -160*e*), consisting of 640 Ala units with 160 Asp units evenly distributed– $(A_2DA_2)_{160}$.

For polypeptides, the CHARMM36 force field was used [26-27]. Noncovalent interactions with a gold nanospheroid were described by the Lennard-Jones potential parameterized in [28], which is widely used in studying the adsorption of molecules on the surface of a gold nanoparticle [29–33]. The van der Waals potential was cut off at 1.2 nm using a smoothing function between 1.0 and 1.2 nm. Electrostatic interactions were calculated directly at a distance of 1.2 nm, and at a larger distance the particle-mesh Ewald method (PME) [34] was used with a grid step of 0.11 nm. The entire nanosystem was placed in a cube with 24 nm edges filled with TIP3P water molecules [35]. To control the obtaining of equilibrium conformations, the change in the root mean square distance between polypeptide atoms in different conformations (RMSD) was monitored. MD simulation was carried out at a constant temperature at 900 K with a subsequent decrease to 300 K. The length of the time trajectory reached 20 ns.

To obtain starting conformations, MD simulation of generally neutral polyampholytic polypeptides (P1-P3) was performed on the neutral surface of a gold nanorod, and to obtain starting conformations of negatively charged polypeptides (numbered P4-P5), MD simulation was performed on the positively charged surface of gold nanorod, in which each surface atom had a partial charge equal to +0.1*e*. In all cases, conformational structures were obtained in which the macrochain completely enveloped the nanorod. Three starting conformations were obtained for each polypeptide considered, which were used as starting ones in modeling on the surface of a longitudinally polarized nanorod.

In the case of longitudinal polarization, the cylindrical part of the metal nanorod remains neutral. Therefore, the local electric field was set through a change in the charges of atoms on the surface of spherical hemispheres located at the ends of the nanorod, where the induced charges were distributed according to the cosine law between the normal to the surface and the direction of the electric field, codirectional with the axis of the nanorod [23]. The following values of the induced dipole moment of the longitudinally polarized nanorod were obtained: $p_{0.25} \approx 11.5$, $p_{0.5} \approx 23$, and $p_{1.0} \approx 46$ kDa. At these values of the dipole moment of the nanorod, the atoms at the pole of its positively charged hemisphere had partial charges: +0.25*e*, +0.5*e* and +1*e*, respectively.

Based on the results of MD simulation for all obtained conformations, the radial distributions of the average density of polypeptide atoms on the surface of the terminal hemispheres of the nanorod and in the middle of the central cylindrical part in a layer 2 nm wide relative to the nanorod axis, as well as the distributions of the linear density of polypeptide atoms along the nanorod axis, were calculated.

5. Results of MD simulation

5.1 Conformational structure of polyampholytic polypeptides on the surface of a longitudinally polarized spherocylinder

Figure 7a shows the conformational structure of polyampholytic polypeptide P2 obtained from MD simulations on the surface of an unpolarized gold nanorod. It can be seen that the macromolecular chain completely envelops the gold nanorod. Similar conformations have been obtained for other polyampholytic polypeptides. Figure 8 (curves 1) shows the radial distributions of the density of polypeptide atoms at the end of the simulation on the surface of a non-polarized neutral nanoparticle. Both in the terminal spherical part (Fig. 8a) of the nanorod and in its central cylindrical part (Fig. 2b), a characteristic distribution of the density of polypeptide atoms with a peak near the surface is formed.

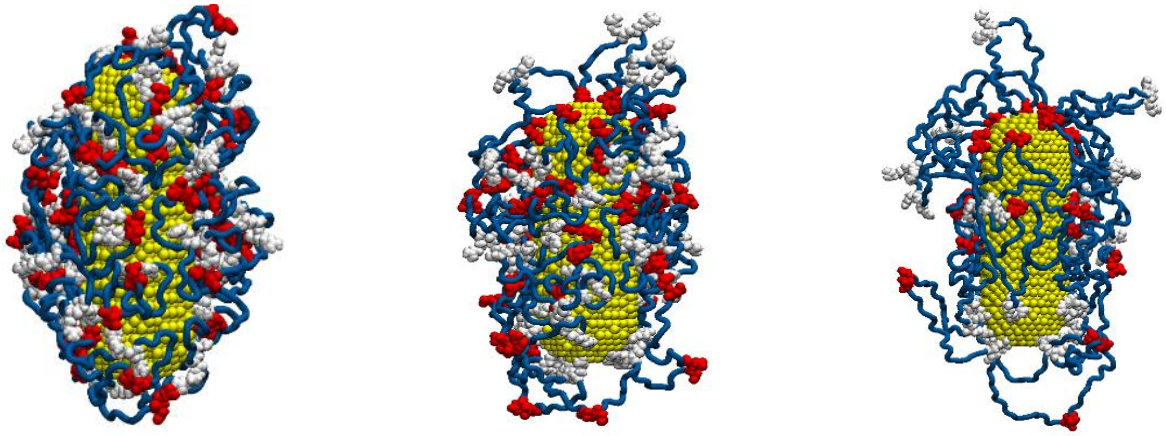

a) *b)* *c)*

Fig.7. Conformational structure of polypeptide P2 after MD simulation on an unpolarized (a) and polarized (b) gold nanorod with a dipole moment of $p_{0.5}$, as well as the conformation of polypeptide P3 (c) on a nanorod polarized with a dipole moment of $p_{1.0}$ (the dipole moment is directed from below - up, the blue tube is the Ala links, the Asp links are shown in red, and the Arg links are white).

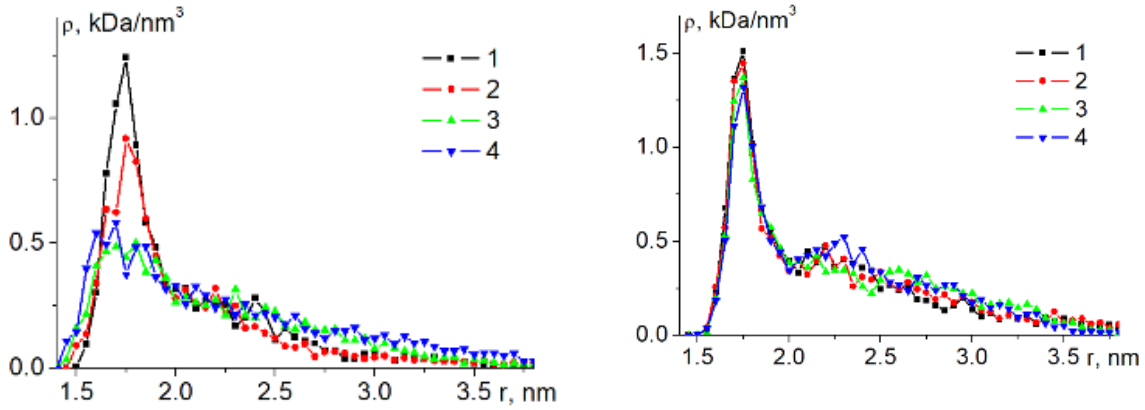

a) b)

Fig.8. Radial distributions of the atomic density of polypeptides P2 (a) and P3 (c) in the region of the upper (Fig. 7) terminal hemisphere (a) of the gold nanorod, as well as in the central region of the cylindrical part of the nanorod (b) at the end of MD simulation at different values of the dipole moment of the nanorod: 1 – 0, 2 - $p_{0.25}$, 3- $p_{0.5}$, 4 - $p_{1.0}$.

As the dipole moment of the longitudinally polarized nanorod increased, the conformational structure of the adsorbed polyampholyte macromolecules changed significantly (Figs. 7b and 7c). At the ends of the gold nanorod, due to the induced electric charges, repulsion of similarly charged units occurred in relation to the surface charge of the terminal hemispheres from the nanorod. This led to elongation of the loops of the polyampholyte macrochain and swelling of the polyampholyte edge at the ends of the nanorod. The radial

distributions of the atomic density of polyampholytic polypeptides obtained at the end of the MD simulation on the surface of a longitudinally polarized nanorod (Fig. 8a) show that as the dipole moment of the nanorod increases, there is a significant decrease in the radial distribution curves of the polypeptide atoms in the terminal spherical region of the nanorod. This decrease in the density of macrochain atoms indicates that the macromolecular edge at the ends of the nanorod swells significantly.

In addition, despite the fact that the central cylindrical part of the nanorod remained neutral, some of the charged units are displaced from it to the charged terminal hemispheres due to the rearrangement of the conformational structure of the polyampholyte at the ends of the longitudinally polarized nanorod. Therefore, in the central cylindrical part of the nanorod, a slight decrease in the radial distribution curves of the atomic density of polyampholytic polypeptides is observed as the dipole moment of the nanorod increases (Fig. 8b).

5.2 Conformational structure of uniformly charged polypeptides on the surface of a longitudinally polarized spherocylinder

In the case of MD simulation of uniformly charged polypeptides, as the dipole moment of the gold nanorod increased, the macrochain units gradually shifted towards the oppositely charged end of the nanorod. Figure 9a shows that when the dipole moment of the nanorod is equal to $p_{0.25}$, the lower negatively charged end of the nanorod is partially exposed, which in the starting conformation was completely enveloped by the P5 polypeptide. With a further increase in the dipole moment to $p_{0.5}$, the lower terminal hemisphere of the nanorod turned out to be completely exposed (Fig. 9b), and at $p_{1.0}$ the macrochain shifted even higher towards the positively charged end of the nanorod (Fig. 9c). Moreover, due to the fact that the central cylindrical part of the nanorod is neutral, the displacement of the charged macrochain after exposure of the lower terminal hemisphere is very weak. Most of the cylindrical part turns out to be covered with macrochain links, in contrast to the case of a polarized elongated gold nanospheroid [19, 21]. This displacement is caused by the displacement of the charged links of the macrochain to the oppositely charged terminal hemisphere, and this is prevented by the van der Waals forces of attraction to the cylindrical part and forces of an entropic nature [24].

This can be seen in the distributions of the linear density of atoms of the P5 polypeptide (Fig. 10a) along the axis of the nanorod depending on the value of its dipole moment. It can be seen that the greater the value of the dipole moment of the gold nanorod, the stronger the shift of the profile in the positive direction of the *z* axis, which coincides with the direction of the dipole moment of the nanorod.

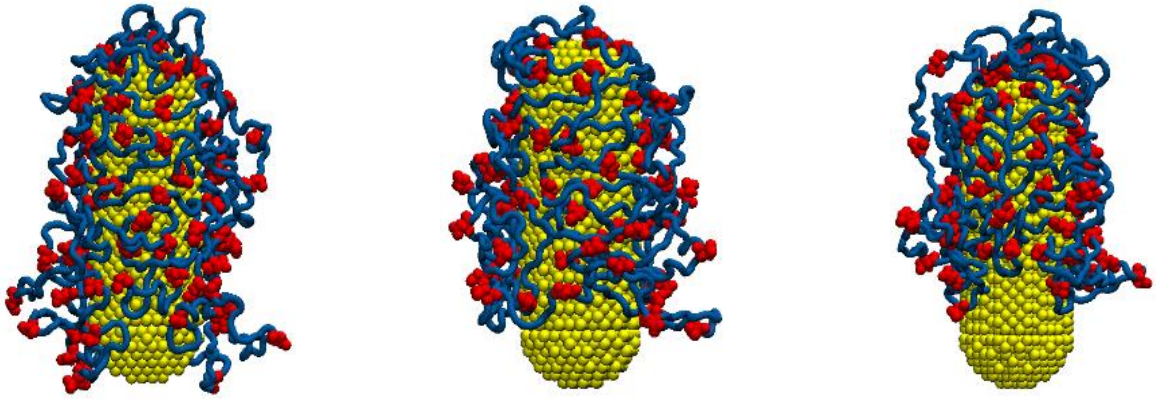

a) *b)* *c)*

Fig.9. Conformations of polypeptide P5 at the end of MD simulation on the surface of a longitudinally polarized gold nanorod (the dipole moment is directed upward) at different values of the dipole moment of the nanorod: $p_{0.25}$ (a), $p_{0.5}$ (b), $p_{.1.0}$ (c) (blue tube - Ala links, Asp links are shown in red).

In addition, in the upper (Fig. 9) positively charged spherical part of the nanorod, as its dipole moment increases, the macromolecular edge of the negatively charged macromolecule swells. This can be seen in the graphs of the radial distributions of the density of atoms of the P5 polypeptide (Fig. 10b) depending on the value of the dipole moment of the nanorod. As the dipole moment of the nanorod increases, a decrease in the radial density distribution curves of a uniformly charged polypeptide is observed (Fig. 10).

This swelling of the edge is due to the fact that as the dipole moment of the nanorod increases, an increasingly greater electrical charge is induced at its positive end, which leads to a displacement of the negative amino acid residues of the polypeptide there.

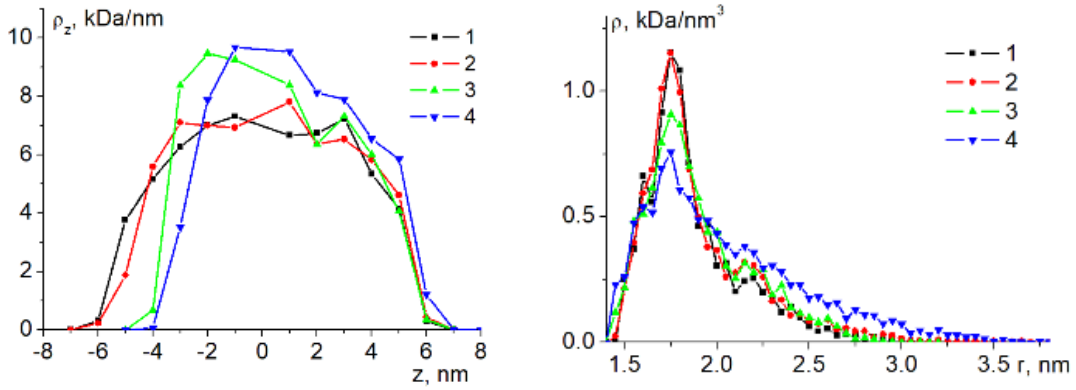

a) *b)*

Fig.10. Distributions of the linear density of atoms of polypeptide P5 (a) along the axis of the nanorod, as well as radial distributions of the density of atoms of polypeptide P5 (b) in the region of the upper (Fig. 9) terminal hemisphere at the end of MD simulation at different values of the dipole moment of the nanorod: 1 – 0, 2 - $p_{0.25}$, 3- $p_{0.5}$, 4 - $p_{1.0}$.

Negative charged amino acid residues Asp gradually fills most of the surface of the terminal positively charged hemisphere, displacing the neutral amino acid residues Ala located between them in the macrochain. And this leads to the formation of macrochain loops, which are formed only by fragments of neutral units, in contrast to the loops of polyampholytic polypeptides (Fig. 7b and 7c).

6. Conclusion

Thus, the work presents an analytical version of the mathematical model of the conformational structure of a polyampholyte and polyelectrolyte macromolecule formed on an elongated nanospheroid in a longitudinal electric field with approximation of the spherocylinder by an elongated spheroid when calculating the characteristics of the resulting field. This model, which takes into account the separated Boltzmann and entropy factors in the density distribution of units, makes it possible to describe the conformational changes of a polymer chain adsorbed on the surface of a cylindrical nanorod with spherical ends in an external electric field without a significant loss of accuracy using simpler expressions than those previously obtained in [18-19] for an elongated nanospheroid. Calculations of radial-angular distributions of unit density based on the proposed model showed significant differences in the response of the distributions to the action of an external electric field polarizing the spherocylinder for polyelectrolytes and polyampholytes. The independent molecular dynamics simulation carried out in the work, in turn, showed that on the surface of a longitudinally polarized gold nanorod, consisting of a central cylindrical part and terminal hemispherical parts, significant conformational changes occur in both generally neutral polyampholyte and uniformly charged macrochains.

Upon adsorption of polyampholyte macromolecules, a dumbbell-shaped macromolecular edge is formed, loose at the ends of the longitudinally polarized nanorod and dense in its central cylindrical part, which is generally similar to the polyampholyte edge on the surface of an elongated spheroidal gold nanoparticle polarized along the major axis. But at the same time, the dumbbell-shaped polyampholyte edge on the surface of a longitudinally polarized nanorod has clearer shapes associated with a clear division into a neutral uncharged cylindrical region and charged terminal hemispheres, in contrast to an elongated polarized gold nanospheroid [21], where the surface density of induced charges was equal to zero only at the equator.

In the case of uniformly negatively charged polypeptides adsorbed on the surface of a longitudinally polarized nanorod, the macromolecular edge gradually shifted to the positively charged hemisphere of the nanorod, swelling there due to the high concentration of charged units on the surface. But in contrast to an elongated spheroidal gold nanoparticle [19, 21], polarized along the major axis, most of the macrochain links remained on the extended neutral cylindrical part of the longitudinally polarized nanorod.

Thus, such control of the shape of the macromolecular edge of polyelectrolyte macromolecules on the surface of a gold nanorod polarized in the longitudinal direction under the influence of an external electric

field can find application in creating and improving the characteristics of sensitive elements of measuring nanoelectronics and nanomaterials, as well as in creating nanoprobes with controlled characteristics for biomedical applications.

Conflict of interest statement

The authors declare that they have no conflict of interest in relation to this research, whether financial, personal, authorship or otherwise, that could affect the research and its results presented in this paper.

CRediT author statement:

Kucherenko M.G.: Conceptualization, Methodology, Investigation, Writing - Original Draft; Kruchinin N.Yu.: Conceptualization, Methodology, Software, Investigation, Writing - Original Draft; Neyasov P.P.: Methodology, Software, Investigation, Writing - Original Draft.

The final manuscript was read and approved by all authors.

Acknowledgments

This work was supported by the Ministry of Science and Higher Education of the Russian Federation within the framework of project no. FSGU-2023-0003.

References

1 Lenjani S.V., Mayer M., Wang R., Dong Y., Fery A., Sommer J., Rossner C. (2022) Importance of electrostatic forces in supracolloidal self-assembly of polymer-functionalized gold nanorods. *J. Phys. Chem. C.*, 126, 14017 – 14025. DOI: 10.1021/acs.jpcc.2c04930.

2 Vedhanayagam M., Andra S., Muthalagu M., Sreeram K.J. (2022) Influence of functionalized gold nanorods on the structure of cytochrome –c: an effective bio-nanoconjugate for biomedical applications. *Inorganic Chemistry Communications*, 146, 110182. DOI: 10.1016/j.inoche.2022.110182.

3 Chakraborty K., Biswas A., Mishra S., Mallick A.M., Tripathi A., Jan S., Roy R.S. (2023) Harnessing peptide-functionalized multivalent gold nanorods for promoting enhanced gene silencing and managing breast cancer metastasis. *ACS Appl. Bio Mater.*, 6, 458–472. DOI: 10.1021/acsabm.2c00726.

4 Dong X., Yu P., Zhao J., Wu Y., Ali M., El-Sayed M.A., Wang J. (2023) Structural Dynamics of (RGD)4PGC peptides in solvated and au nanorod surface-bound forms examined by ultrafast 2d IR Spectroscopy. *J. Phys. Chem. C*, 127, 3532–3541. DOI: 10.1021/acs.jpcc.2c07830.

5 Wei W., Bai F., Fan H. (2019) Oriented gold nanorod arrays: self-assembly and optoelectronic applications. *Angewandte Chemie International Edition*, 58, 11956–11966. DOI: 10.1002/anie.201902620.

6 Halder K., Sengupta P., Chaki S., Saha R., Dasgupta S. (2023) Understanding conformational changes in human serum albumin and its interactions with gold nanorods: do flexible regions play a role in corona formation? *Langmuir*, 39, 1651–1664. DOI: 10.1021/acs.langmuir.2c03145.

7 Trofymchuk K., Kołątaj K., Glembockyte V., Zhu F., Acuna G.P., Liedl T., Tinnefeld P. (2023) Gold Nanorod DNA Origami Antennas for 3 Orders of Magnitude Fluorescence Enhancement in NIR. *ACS Nano*, 17, 1327–1334. DOI: 10.1021/acsnano.2c09577.

8 Han S., Wang J.T., Yavuz E., Zam A., Rouatbi N., Utami R.N., Liam-Or R., Griffiths A., Dickson W., Sosabowski J., Al-Jamal K.T. (2023) Spatiotemporal tracking of gold nanorods after intranasal administration for brain targeting. *Journal of Controlled Release*, 357, 606-619. DOI: 10.1016/j.jconrel.2023.04.022.

9 Pal S., Koneru J.K., Andreou C., Rakshit T., Rajasekhar V.K., Wlodarczyk M., Healey J.H., Kircher M.F., Mondal J. (2022) DNA-Functionalized Gold Nanorods for Perioperative Optical Imaging and Photothermal Therapy of Triple-Negative Breast Cancer. *ACS Appl. Nano Mater.*, 5, 9159–9169. DOI: 10.1021/acsanm.2c01502.

10 Hosseinniya S., Rezayan A.H., Ghasemi F., Malekmohamadi M., Taheri R.A., Hosseini M., Alvandi H. (2023) Fabrication and evaluation of optical nanobiosensor based on localized surface plasmon resonance (LSPR) of gold nanorod for detection of CRP. *Analytica Chimica Acta*, 1237, 340580. DOI: 10.1016/j.aca.2022.340580.

11 Chang Y., Wang Q., Xu W., Huang X., Xu X., HanF.Y., Qiao R., Ediriweera G.R., Peng H., Fu C., Liu K., Whittaker A.K. (2022) Low-fouling gold nanorod theranostic agents enabled by a sulfoxide polymer coating. *Biomacromolecules*, 23, 3866–3874. DOI: 10.1021/acs.biomac.2c00696.

12 Zhao H., Jiang T., Yi L., Tang L. (2021) DNA sequences-mediated fine-tuning of nanostructures and their plasmonic properties over gold nanorods. *Optik*, 228, 166137. DOI: 10.1016/j.ijleo.2020.166137.

13 Li M., Lu D., You R., Shen H., Zhu L., Lin Q., Lu Y. (2022) Surface-enhanced Raman scattering biosensor based on self-assembled gold nanorod arrays for rapid and sensitive detection of tyrosinase. *J. Phys. Chem. C*, 126, 12651–12659. DOI: 10.1021/acs.jpcc.2c03408.

14 Kruchinin N.Yu., Kucherenko M.G. (2020) Molecular-Dynamics Simulation of Rearrangements in the Conformational Structure of Polyampholytic Macromolecules on the Surface of a Polarized Metal Nanoparticle. *Colloid Journal*, 82, 136-143. DOI: 10.1134/S1061933X20020088.

15 Kruchinin N.Yu., Kucherenko M.G. (2021) Rearrangements in the conformational structure of polyampholytic polypeptides on the surface of a uniformly charged and polarized nanowire: Molecular dynamics simulation. *Surfaces and Interfaces*, 27, 101517. DOI: 10.1016/j.surfin.2021.101517.

16 Kucherenko M.G., Kruchinin N.Yu., Neyasov P.P. (2022) Modeling of conformational changes of polyelectrolytes on the surface of a transversely polarized metal nanowire in an external electric field. *Eurasian Physical Technical Journal*, 19, 19-29. DOI: 10.31489/2022No2/19-29.

17 Kruchinin N.Yu., Kucherenko M.G. (2021) Molecular dynamics simulation of conformational rearrangements in polyelectrolyte macromolecules on the surface of a charged or polarized prolate spheroidal metal nanoparticle. *Colloid Journal*, 83, 591-604. DOI:10.1134/S1061933X21050070.

18 Kruchinin N.Yu., Kucherenko M.G. (2021) Modeling the conformational rearrangement of polyampholytes on the surface of a prolate spheroidal metal nanoparticle in alternating electric field. *High Energy Chemistry,* 55, 442-453. DOI:10.1134/S0018143921060084.

19 Kruchinin N.Yu., Kucherenko M.G. (2022) Molecular dynamics simulation of the conformational structure of uniform polypeptides on the surface of a polarized metal prolate nanospheroid with varying pH. *Russian Journal of Physical Chemistry A*, 96, 624-632. DOI:10.1134/S0036024422030141.

20 Kruchinin N.Y., Kucherenko M.G. (2022) Conformational changes of polyelectrolyte macromolecules on the surface of charged prolate metal nanospheroid in alternating electric field. *Polymer Science Series A*, 64, 240–254. DOI:10.1134/S0965545X2203004X.

21 Kruchinin N.Yu., Kucherenko M.G. (2022) Modeling of electrical induced conformational changes of macromolecules on the surface of metallic nanospheroids. *Materials Today: Proceedings*, 71, Part 1, 18-30. DOI:10.1016/j.matpr.2022.07.139.

22 Kruchinin N.Y., Kucherenko M.G. (2023) Rearrangements in the Conformational Structure of Polyelectrolytes on the Surface of a Flattened Metal Nanospheroid in an Alternating Electric Field. *Colloid Journal*, 85, 44-58. DOI:10.1134/S1061933X22600440.

23 Landau L.D., Pitaevskii L.P., Lifshitz E.M. (1984), *Electrodynamics of Continuous Media*, 2nd Edition, Elsevier Ltd., 460.

24 Grosberg A.Y., Khokhlov A.R. (1994) *Statistical Physics of Macromolecules*. AIP Press, New York. 347.

25 Phillips J.C., Braun R., Wang W., Gumbart J., Tajkhorshid E., Villa E., Chipot C., Skeel R.D., Kale L, Schulten K. (2005) Scalable molecular dynamics with NAMD. *J Comput Chem.*, 26, 1781-1802. DOI:10.1002/jcc.20289.

26 MacKerell A.D. Jr., Bashford D., Bellott M., Dunbrack Jr. R.L., Evanseck J.D., Field M.J., Fischer S., Gao J., Guo H., Ha S., Joseph-McCarthy D., Kuchnir L., Kuczera K., Lau F.T.K., Mattos C., Michnick S., Ngo T., Nguyen D.T., Prodhom B., Reiher III W.E., Roux B., Schlenkrich M., Smith J.C., Stote R., Straub J., Watanabe M., Wiorkiewicz-Kuczera J., Yin D., Karplus M. (1998) All-atom empirical potential for molecular modeling and dynamics studies of proteins *J. Phys. Chem. B.*,102, 3586-3616. DOI:10.1021/jp973084f.

27 Huang, J., Rauscher, S., Nawrocki, G., Ran T., Feig M., de Groot B.L., Grubmüller H., MacKerell Jr. A.D. (2016) CHARMM36m: an improved force field for folded and intrinsically disordered proteins. *Nature Methods*, 14. 71-73. DOI: 10.1038/nmeth.4067.

28 Heinz H., Vaia R.A., Farmer B.L., Naik R.R. (2008) Accurate simulation of surfaces and interfaces of face-centered cubic metals using 12−6 and 9−6 Lennard-Jones potentials. *J. Phys. Chem. C.*, 112, 17281-17290. DOI: 10.1021/jp801931d.

29 Cappabianca R., De Angelis P., Cardellini A., Zhuang Y., Hernandez R. (2022) Assembling biocompatible polymers on gold nanoparticles: toward a rational design of particle shape by molecular dynamics. *ACS Omega*, 7, 42292-42303. DOI: 10.1021/acsomega.2c05218.

30 Wei X., Harazinska E., Zhao Y., Zhuang Y., Hernandez R. (2022) Thermal transport through polymer-linked gold nanoparticles. *The Journal of Physical Chemistry C*., 126, 18511-18519. DOI: 10.1021/acs.jpcc.2c05816.

31 Chew A.K., Pedersen J.A., Van Lehn R.C. (2022) Predicting the physicochemical properties and biological activities of monolayer-protected gold nanoparticles using simulation-derived descriptors. *ACS Nano*, 16, 6282-6292. DOI: 10.1021/acsnano.2c00301.

32 Jia H., Zhang Y., Zhang C., Ouyang M., Du S. (2023) Ligand–ligand-interaction-dominated self-assembly of gold nanoparticles at the oil/water interface: an atomic-scale simulation. *The Journal of Physical Chemistry B*, 127, 2258-2266. DOI:10.1021/acs.jpcb.2c07937.

33 Wang X., Ham S., Zhou W., Qiao R. (2023) Adsorption of rhodamine 6G and choline on gold electrodes: a molecular dynamics study. *Nanotechnology*, 34, 025501. DOI: 10.1088/1361-6528/ac973b.

34 Darden T., York D., Pedersen L. (1993) Particle mesh Ewald: An N·log(N) method for Ewald sums in large systems *J. Chem. Phys*., 98, 10089-10092. DOI: 10.1063/1.464397.

35 Jorgensen W.L., Chandrasekhar J., Madura J.D., Impey R.W., Klein M.L. (1983) Comparison of simple potential functions for simulating liquid water. *J. Chem. Phys*., 79, 926-935. DOI:10.1063/1.445869.

AUTHORS' INFORMATION

Kucherenko, Michael Gennadievich - Doctor of phys.-math. sciences, Professor, Director of the Center for Laser and Informational Biophysics, Orenburg State University, Orenburg, Russia; Scopus Author ID: 7003581468; ORCID iD: 0000-0001-8821 -2427, clibph@yandex.ru

Kruchinin, Nikita Yurevich - Doctor of phys.-math. sciences, Associate Professor, Department of radiophysics and electronics, Orenburg State University, Orenburg, Russia; Scopus Author ID: 35170029600; ORCID iD: 0000-0002-7960-3482; kruchinin_56@mail.ru

Neyasov, Petr P. – Master (Sci.), Head of the Laboratory of Nanostructure Synthesis, Orenburg State University, Orenburg, Russia; Scopus Author ID: 57222337052; ORCID iD: 0000-0002-7133-8741; nejapetr@yandex.ru